Bone Reports 9 (2018) 61–73

Contents lists available at ScienceDirect

Bone Reports

journal homepage: www.elsevier.com/locate/bonr

Loss of RANKL in osteocytes dramatically increases cancellous bone mass in the osteogenesis imperfecta mouse (oim)

Sarah M. Zimmerman[a], Melissa E. Heard-Lipsmeyer[a], Milena Dimori[a], Jeff D. Thostenson[b], Erin M. Mannen[e], Charles A. O'Brien[c,d,e], Roy Morello[a,e,f,*]

[a] Department of Physiology & Biophysics, University of Arkansas for Medical Sciences, Little Rock, AR, United States of America
[b] Department of Biostatistics, University of Arkansas for Medical Sciences, Little Rock, AR, United States of America
[c] Center for Osteoporosis and Metabolic Bone Diseases, University of Arkansas for Medical Sciences, Little Rock, AR, United States of America
[d] Central Arkansas Veterans Healthcare System, Little Rock, AR, United States of America
[e] Department of Orthopaedic Surgery, University of Arkansas for Medical Sciences, Little Rock, AR, United States of America
[f] Division of Genetics, University of Arkansas for Medical Sciences, Little Rock, AR, United States of America

ARTICLE INFO

Keywords:
Osteocyte
RANKL
Osteogenesis imperfecta
Bone fragility

ABSTRACT

Osteogenesis imperfecta (OI) is characterized by osteopenia and bone fragility, and OI patients during growth often exhibit high bone turnover with the net result of low bone mass. Recent evidence shows that osteocytes significantly affect bone remodeling under physiological and pathological conditions through production of osteoclastogenic cytokines. The receptor activator of nuclear factor kappa-B ligand (RANKL) produced by osteocytes for example, is a critical mediator of bone loss caused by ovariectomy, low-calcium diet, unloading and glucocorticoid treatment. Because OI bone has increased density of osteocytes and these cells are embedded in matrix with abnormal type I collagen, we hypothesized that osteocyte-derived RANKL contributes to the OI bone phenotype. In this study, the conditional loss of RANKL in osteocytes in oim/oim mice (oim-RANKL-cKO) resulted in dramatically increased cancellous bone mass in both the femur and lumbar spine compared to oim/oim mice. Bone cortical thickness increased significantly only in spine but ultimate bone strength in the long bone and spine was minimally improved in oim-RANKL-cKO mice compared to oim/oim mice. Furthermore, unlike previous findings, we report that oim/oim mice do not exhibit high bone turnover suggesting that their low bone mass is likely due to defective bone formation and not increased bone resorption. The loss of osteocyte-derived RANKL further diminished parameters of formation in oim-RANKL-cKO. Our results indicate that osteocytes contribute significantly to the low bone mass observed in OI and the effect of loss of RANKL from these cells is similar to its systemic inhibition.

1. Introduction

Osteogenesis imperfecta (OI) is the most common congenital skeletal fragility disorder, affecting approximately 6–7 per 100,000 people worldwide (Genetics Home Reference, n.d.). Also known as brittle bone disease, OI is mainly characterized by fragile bones and low bone mass, and most cases (around 85%) are caused by dominant mutations in the type I collagen genes, *COL1A1* or *COL1A2* (*Marini* et al., *2017*). At the bone tissue level, the disease is generally characterized by low bone mass and a high fracture rate, with significant alterations in bone modeling and endochondral ossification, and bone remodeling (Rauch et al., 2000). At the cellular level, osteoblasts, the bone forming cells, and their function have been the main focus of research in OI pathogenesis. This is justified by the fact that osteoblasts are the key producers of bone matrix (osteoid) whose main component is type I collagen. A defective type I collagen can dramatically impact bone matrix quality and its proper mineralization, and when incorrectly folded can also be retained intracellularly and cause ER stress, ultimately resulting in dysfunctional osteoblasts that deposit less bone which is also brittle. Osteoclasts are likely indirectly affected by a defective type I collagen and are often present in higher number on OI bone surfaces compared to healthy controls as shown by a bone histomorphometric study of a pediatric cohort of patients with OI type I, III and IV (Rauch et al., 2000). This study showed a marked increase in all bone surface-based formation and resorption indices, indicating a state of high bone turnover which was also reported by others (Rauch et al.,

* Corresponding author at: Department of Physiology & Biophysics, University of Arkansas for Medical Sciences, 4301 W. Markham St., #505, Little Rock, AR 72205-7199, United States of America.
E-mail address: rmorello@uams.edu (R. Morello).

https://doi.org/10.1016/j.bonr.2018.06.008
Received 22 March 2018; Received in revised form 30 May 2018; Accepted 29 June 2018
Available online 02 July 2018

2000; Baron et al., 1983; Braga et al., 2004). Interestingly, while the amount of bone turned over in each remodeling cycle appears to be decreased in OI, the activation frequency, defined as the number of remodeling units per bone surface per time unit, is markedly elevated (up to 60% more in OI type I compared to controls) (Rauch et al., 2000). The third type of bone cells, the osteocytes, are long-lived compared to osteoblasts and osteoclasts and are the most numerous cells in the adult skeleton. Studies showed that osteocytes affect osteoblast and osteoclast formation and function through the local synthesis and secretion of growth factors and cytokines such as WNT ligands and Sclerostin, but also RANKL, an essential cytokine for osteoclastogenesis, and osteoprotegerin (OPG), an inhibitor of RANKL signaling (Bellido, 2014; van Bezooijen et al., 2004; Joeng et al., 2017). Importantly, it was recently shown that osteocytes are the most important source of RANKL during bone remodeling (Xiong et al., 2011; Nakashima et al., 2011) and osteocyte-derived RANKL is a critical mediator of the increased bone resorption and bone loss caused by ovariectomy, low-calcium diet, unloading and glucocorticoid treatment (Xiong et al., 2014; O'Brien et al., 2013; Fujiwara et al., 2016; Piemontese et al., 2016). It is known that OI bone exhibits increased density of osteocytes which are embedded in a matrix of altered type I collagen, however how the dysregulation/activity of these cells may potentially contribute to the OI disease phenotype is currently understudied. Because current treatments for OI also aim to decrease bone resorption (for instance using bisphosphonates or the anti-RANKL monoclonal antibody Denosumab), these could be made more effective through a better understanding of the underlying cellular mechanisms.

In this study, we generated a novel mouse model to test our hypothesis that RANKL from osteocytes contributes significantly to the low bone mass and the high bone turnover observed in OI. To do this we mated oim mice ($Col1a2^{oim/oim}$), a widely accepted mouse model of moderate to severe OI (Chipman et al., 1993), with mice carrying a floxed *Tnfsf11* gene (encodes RANKL) and a Cre transgene driven by the *Dmp1* promoter (Xiong et al., 2011; Lu et al., 2007). This mouse (called "oim-RANKL-cKO") is a model for OI but lacks RANKL expression in osteocytes, and therefore enabled us to determine the contribution of osteocyte-produced RANKL to the skeletal phenotype of the oim mouse model.

2. Materials & methods

2.1. Mouse generation and genotyping

The use of laboratory mice was approved by the University of Arkansas for Medical Sciences (UAMS) IACUC committee. Mice were housed in a pathogen free facility with 12-hour light/dark cycle with unlimited access to water and standard chow diet. RANKL-cKO mice ($Tnfsf11l^{Fl/Fl}$; *Dmp1-Cre*) were generated with loxP sites flanking exons 3 and 4 of *Tnfsf11* and a Cre recombinase driven by a construct containing 9.6 kb of the *Dmp1* promoter and 4 kb of *Dmp1* exon 1 on a C57Bl/6 background by Dr. Charles O'Brien (Xiong et al., 2011; Lu et al., 2007). The oim mice ($Col1a2^{oim/+}$) in a pure C57Bl/6 genetic background were obtained from Dr. Charlotte Phillips at the University of Missouri-Columbia, MO (Carleton et al., 2008). The oim mice were maintained in a separate colony and also bred with the RANKL-cKO mice to produce mice with the genotype of interest in three steps, keeping the mice heterozygous for the oim mutation until the final step and always hemizygous for the Cre allele (for schematic see Fig. 1A). The mice were weighed once every week beginning at 5 weeks of age until sacrifice at 13 weeks of age. At sacrifice, the number of femora and tibiae per mouse with fractures were recorded. PCR genotyping was performed with the GoTaq G2 Hot Start Polymerase reagent (cat# M7423 Promega) and a Master Cycler thermocycler (Eppendorf). Protocols for *Rankl-flox* and *Dmp1-Cre* genotyping were described previously (Xiong et al., 2011). To ensure the correct conditional knockout of RANKL, a new genotyping protocol was developed to detect the deletion. Utilizing the primers Forward 5′-CTGGGAGCGCAGGTTAA ATA-3′ (the same forward primer as for *Tnfsf11-flox* genotyping) and Reverse 5′-GAGACATTAGAGCCCGGTCA-3′, this protocol amplifies the genomic DNA region encompassing the entire floxed region of *Tnfsf11* plus approx. 800 bp downstream of that region (Supplementary Fig. 1A). The products of the amplification are a large band (approx. 2.1 kb) for the intact *Tnfsf11-flox* allele or a smaller band (approx. 800 bp) for the recombined *Tnfsf11* allele (Supplementary Fig. 1B).

A new genotyping strategy was developed for detecting the oim mutation, based on the T-ARMS PCR method (Ye et al., 2001). The primers are 5′-ACTGTCTGTCTACAGTGAACGTCTTAA T-3′ outer forward, 5′-GATGTAGATGCATAGAAGACATGGAAGG-3′ outer reverse, 5′-TTCCCATTTTTTTCTATTATACAGAAACAG-3′ inner forward (WT specific), and 5′-AATGATTGTCTTGCCCCATTCATTTTTT-3′ inner reverse (oim specific) which flank the single nucleotide deletion (Supplementary Fig. 1C). These four primers were added to the same master mix for a final concentration of 0.1 μM (outer primers) and 1.0 μM (inner primers). The PCR program is as follows: 94 °C for 2 min, then 30 cycles of 94 °C for 30 s, 60 °C for 30 s, and 72 °C for 30 s, and lastly, 72 °C for 5 min. The products are 440 bp (all genotypes), 303 bp (WT allele) and 195 bp (oim allele) and an example gel image of the results is provided in Supplementary Fig. 1D.

2.2. Micro-CT

Femur and lumbar spine were harvested from 3 month old male and female oim-RANKL-cKO mice and control groups and fixed in 95% ethanol. Micro-CT analysis was performed on a Micro-CT 40 (Scanco Medical AG, Bassersdorf, Switzerland) using a 12 μm isotropic voxel size. For cancellous bone of the femur, the region of interest selected for analysis comprised 200 transverse CT slices representing the entire medullary volume extending 1.24 mm distal to the end of the primary spongiosa with a border lying 100 μm from the cortex. For cancellous bone of the L4 vertebral body, the region of interest for analysis comprised the entire cancellous bone volume. Three-dimensional reconstructions were created by stacking the regions of interest from each two-dimensional slice and then applying a grayscale threshold and Gaussian noise filter (sigma 0.8, support 1, threshold 245) as described (Suva et al., 2008), using a consistent and pre-determined threshold with all data acquired at 55 kVp, 114 mA, and 200 ms integration time. Fractional bone volume (bone volume/tissue volume; BV/TV) and architectural properties of trabecular bone such as trabecular thickness (Tb.Th, μm), trabecular number (Tb.N, mm^{-1}), and connectivity density (Conn. D, mm^{-3}) were calculated using previously published methods (Suva et al., 2008). Femoral cortical geometry was assessed in a region centered at the femoral midshaft. The outer surface of the bone was found automatically using the manufacturer's built-in contouring tool. Total area was calculated by counting all voxels within the contour and bone area by counting all voxels that were segmented as bone. Marrow area was calculated as total area minus bone area. This calculation was performed on all 50 slices (1 slice = 12.5 μm), using the average for the final calculation. The outer and inner perimeter of the cortical midshaft was determined by a three-dimensional triangulation of the bone surface (BS); other cortical parameters were determined as described (Suva et al., 2008). Vertebral cortical bone measurements were made on the ventral side of the L4 vertebral body, encompassing 100 slices from the distal growth plate, or the maximum slices possible between one growth plate and the other. The reporting of micro-CT measurements follows the guidelines of Bouxsein et al. (Bouxsein et al., 2010). Femur length was measured using a digital caliper (Whitworth). Each sample was measured twice and the average of the two measurements was used for data analysis.

2.3. Biomechanics

Femurs from 3 month old male and female oim-RANKL-cKO mice

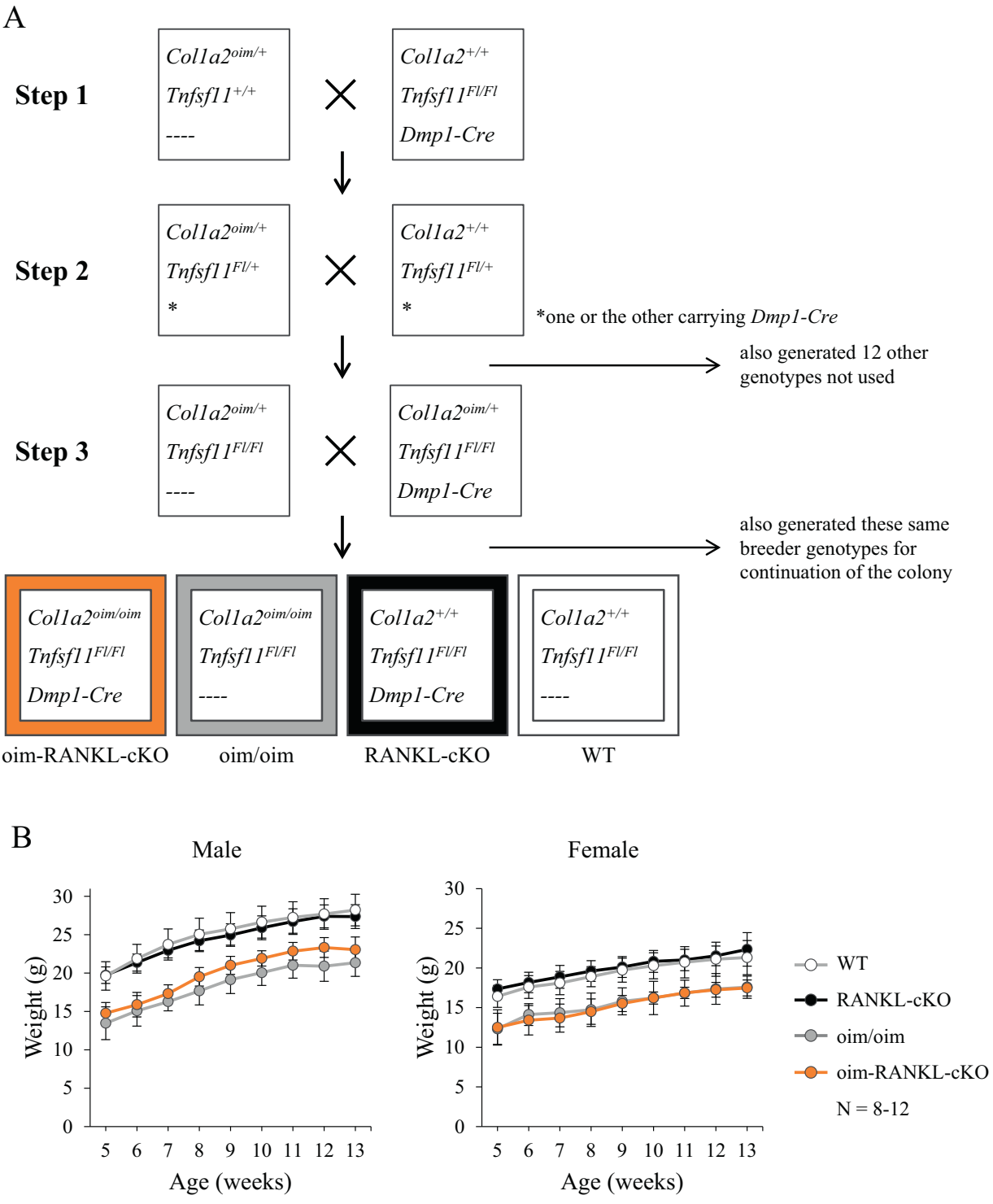

Fig. 1. Generation of oim-RANKL-cKO mice. A. Breeding strategy for the generation of the oim-RANKL-cKO mice and control groups WT, RANKL-cKO, and oim/oim. B. Body weight (in grams) was measured weekly from 5 weeks of age until sacrifice at 13 weeks of age (N = 8–12). The oim-RANKL-cKO and oim/oim groups are significantly lower than the RANKL-cKO and WT groups at every time point, $p < 0.0001$.

and control groups were collected at sacrifice and frozen at −20 °C wrapped in saline-soaked gauze. These femurs (n = 4–6 each sex-genotype group) were utilized in a 3-point bending test on an INSTRON model 5542, with a ramp rate of 1 mm/min and support span of 8.1 mm, and running Bluehill2 software ver. 2.35. Analysis of the data models the bone as a hollow, uniform elliptic cylinder, assumes that this includes cortical bone only, and uses Euler-Bernoulli beam theory. Values for area moment of inertia (I) were derived from micro-CT scans of the contralateral femur of the same mouse. In cases where the contralateral femur was unable to be scanned, the average value of I for all micro-CT scans in that sex-genotype group was used. Elastic modulus, yield stress, and ultimate stress were calculated for each sample. Stress-strain curves were generated from the group average values. Spines utilized for micro-CT from 3 month old female mice (n = 5–6 each genotype) were subsequently dissected (post-fixation) to isolate the L5 vertebral body for use in a vertebral compression test on the Instron

5542 with a ramp rate of 0.5 mm/min. Analysis of the compression data assumes the vertebral body is a solid, uniform elliptic cylinder. Maximum compressive force, strain at maximum load, and elastic modulus were calculated for each sample.

2.4. Histomorphometry

Spines used for micro-CT from 3 month old male oim-RANKL-cKO mice and control groups (n = 6–10) were subsequently utilized for histomorphometry. For the measurement of the bone formation rate, the mice were injected i.p. with 30 mg/kg Alizarin red (alizarin-3-methyliminodiacetic acid, Sigma cat: A3882) and calcein (Sigma cat: C0875) dyes at 7 and 2 days before sacrifice, respectively. Portions of non-decalcified spine encompassing three vertebral bodies were embedded in methylmethacrylate according to standard procedures, sectioned, and stained with anti-TRAP. Unstained sections were used for fluorescent double label analysis. The analysis was performed using a Nikon Eclipse E400 microscope equipped with fluorescent light, an Olympus DP73 camera and OsteoMeasure7 software (OsteoMetrics, Inc.). The entire cancellous bone area of 3 vertebral bodies was used, when possible, for counting osteocyte number (N.Ot), osteoclast number (N.Oc), and osteoclast surface (Oc.S) on the TRAP stained slides. Mineral apposition rate (MAR) and bone formation rate (BFR) were measured on the unstained slides, using the entire cancellous bone area of 2 vertebral bodies. The results are reported using the abbreviations recommended by the American Society for Bone and Mineral Research Histomorphometric Nomenclature Committee (Dempster et al., 2013).

2.5. Measurement of bone resorption markers

Serum samples were collected from the mice at sacrifice and stored at −20 °C until testing. Serum samples were used in the RatLaps CTX-I EIA and TRAcP5b ELISA (immunodiagnostic systems CTX-I REF: AC-06F1 Lot: 33144, TRAcP5b REF: SB-TR103 Lot: 34983) according to the manufacturer's instructions. For measurement of soluble RANKL (sRANKL) and OPG protein in bone marrow supernatant, femur and tibia were dissected from 3 month old WT and oim mice. The epiphyses were removed with scissors and the marrow was collected via centrifugation. The marrow was resuspended in 120 µl PBS, and then centrifuged again. The supernatant was collected, flash frozen in liquid nitrogen and stored at −80 °C until ready to use. The supernatant samples were tested using RANKL and OPG ELISA kits (R&D Systems RANKL Cat: MTR00 Lot: 321723, OPG Cat: MOP00 Lot: 317518) according to the manufacturer's instructions.

2.6. Osteocyte-enriched RNA preparation and real-time PCR

Femur and tibia were processed as detailed above for bone marrow supernatant collection. The cortical bone was flushed thoroughly with PBS and the outer surface was scraped with a scalpel to remove the periosteum. This osteocyte-enriched cortical bone was immediately homogenized in 1 ml TriPure Isolation Reagent (Roche REF11667157001) and processed for RNA extraction according to the manufacturer's instructions until the chloroform separation step. An equal volume of freshly-made, RNase-free 75% ethanol was added to the clear supernatant obtained from the chloroform separation, mixed, and then transferred to an RNeasy Micro column (Qiagen cat# 74004). Digestion with DNase I and elution of RNA was performed according to the manufacturer's instructions. Synthesis of cDNA from the osteocyte-enriched RNA was performed with the Transcriptor First Strand cDNA Synthesis Kit (Roche REF 04379012001), according to the manufacturer's instructions. Real-time PCR was performed to measure *Rankl*, *Opg*, *Ocn*, and *Trap* gene expression, which was normalized using the geometric mean of five housekeeping genes *Gapdh*, *G6pdh*, *Pbgd*, *B2mg* and *Hprt*, using the primers listed in Table 1.

Table 1
Primer sequences used for real-time PCR.

Gene	Primer sequences 5′ to 3′
Tnfsf11 (Rankl)	F - CCCTGAAGGTACTCGTAGCTAAG
	R - GGCTATGTCAGCTCCTAAAGTCAA
Tnfrsf11b (Opg)	F - CCAACAGTTTATCCAGCTGTCATGTC
	R - CCATATTCAAAGAGATCCAATGGAGT
Bglap, Bglap2 and 3 (Ocn)	F - ACCCTGGCTGCGCTCTGTCTCT
	R - GATGCGTTTGTAGGCGGTCTTCA
Acp5 (Trap)	F - AGAGTCCTGCTTGTCCGCTAA
	R - GATCAGTTGGTGTGGGCATACTTC
Gapdh	F - GCAAGAGAGGCCCTATCCCAA
	R - CTCCCTAGGCCCCTCCTGTTATT
G6pdh	F - AGATTGATCGAGAAAAGCC
	R - AGCTGGGTTTACTGGTG
Pbgd	F - GTGATGAAAGATGGGCAA
	R - TCTTGGCTCCTTTGTTGA
B2mg	F - GGTCTTTCTGGTGCTTGTC
	R - CGTATGTATCAGTCTCAGT
Hprt	F - TCTGGTAGATTGTCGCTTATCTTG
	R - TAGATGCTGTTACTGATAGGAAATCGAG

2.7. Statistical analysis

The data collected from oim and WT mice were analyzed using the Student's *t*-test or by Wilcoxon Rank-sum test for non-normal data, to compare the two groups. Body weight data was analyzed with a Repeated Measure model. All other data was analyzed using 2-way ANOVA followed by Tukey's post-hoc test. Transformations were used to achieve normality and equal variance assumptions. If either assumption was still violated, data was ranked and then analyzed non-parametrically. Femur biomechanical parameters were analyzed by 3-way ANOVA to account for sex differences. Two-sample tests, Repeated Measures model, and 2-way and 3-way ANOVAs were all done using SAS v9.4 (Cary, NC). Fracture prevalence was analyzed with the "N-1" modified Chi-squared test for comparing proportions freely available at the MEDCALC statistical software website (medcalc.org/calc/comparison_of_proportions), and the 95% confidence interval was calculated using the free online calculator from GraphPad (graphpad.com/quickcalcs/confInterval1). Body weight, protein concentration, and gene expression data is reported as mean ± standard deviation, fracture prevalence is reported as percent with fracture and the 95% confidence interval, and the remainder of the data is displayed in box plots where the lower and upper limits of the box indicate the first and third quartiles, the center line indicates the median, and the whiskers indicate the minimum and maximum values. p values < 0.05 were considered statistically significant and reported as such.

2.8. Ethics statement

All animal work (i.e. on rodents) performed in this study was conducted in accordance to local, State and US Federal regulations. The UAMS IACUC approved the animal protocol (AUP#3466 entitled "Unrecognized role of osteocytes in osteogenesis imperfecta") describing all the procedures performed in this study. Mice were euthanized to harvest relevant tissues according to the recommendations of the Guide for Care and Use of Laboratory Animals (8th Edition).

3. Results

3.1. Generation of oim-RANKL-cKO mouse model and initial characterization

Heterozygous male oim mice (*Col1a2*$^{oim/+}$) were mated with female RANKL-cKO mice (*Tnfsf11*$^{Fl/Fl}$; *Dmp1-Cre*) and the resulting offspring were bred further so that, over a total of 3 generations, we generated mice with the following desired genotypes (Fig. 1A): *Col1a2*$^{oim/oim}$;

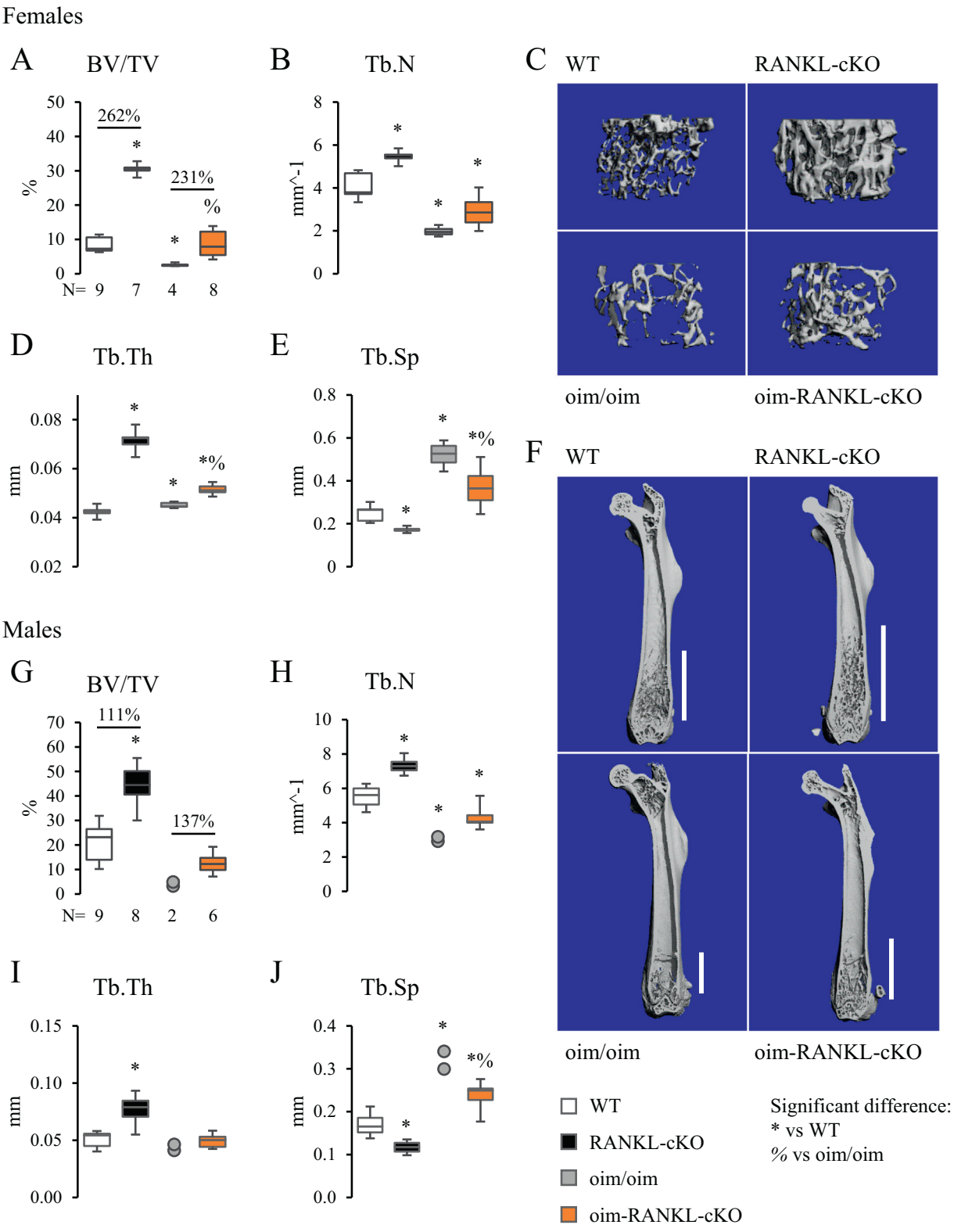

Fig. 2. Micro-CT analysis of static cancellous bone parameters in the distal femur. Trabecular bone parameters from micro-CT analysis of femur from female (A–F) and male (G–J) 3 month old mice including bone volume over tissue volume (BV/TV), trabecular number (Tb.N), trabecular thickness (Tb.Th), and trabecular separation (Tb.Sp). The N is indicated below the graphs. Because of the small number of usable specimens in the male oim/oim group (N = 2, due to fractures present in other specimens), the data for this group is displayed as individual data points instead of a box-and-whiskers plot. C, F. Representative 3D reconstructions of trabecular bone in distal femur and of whole femur, respectively, from female mice of each genotype. The white bars in F indicate the extent of cancellous bone from the growth plate into the diaphyseal area.

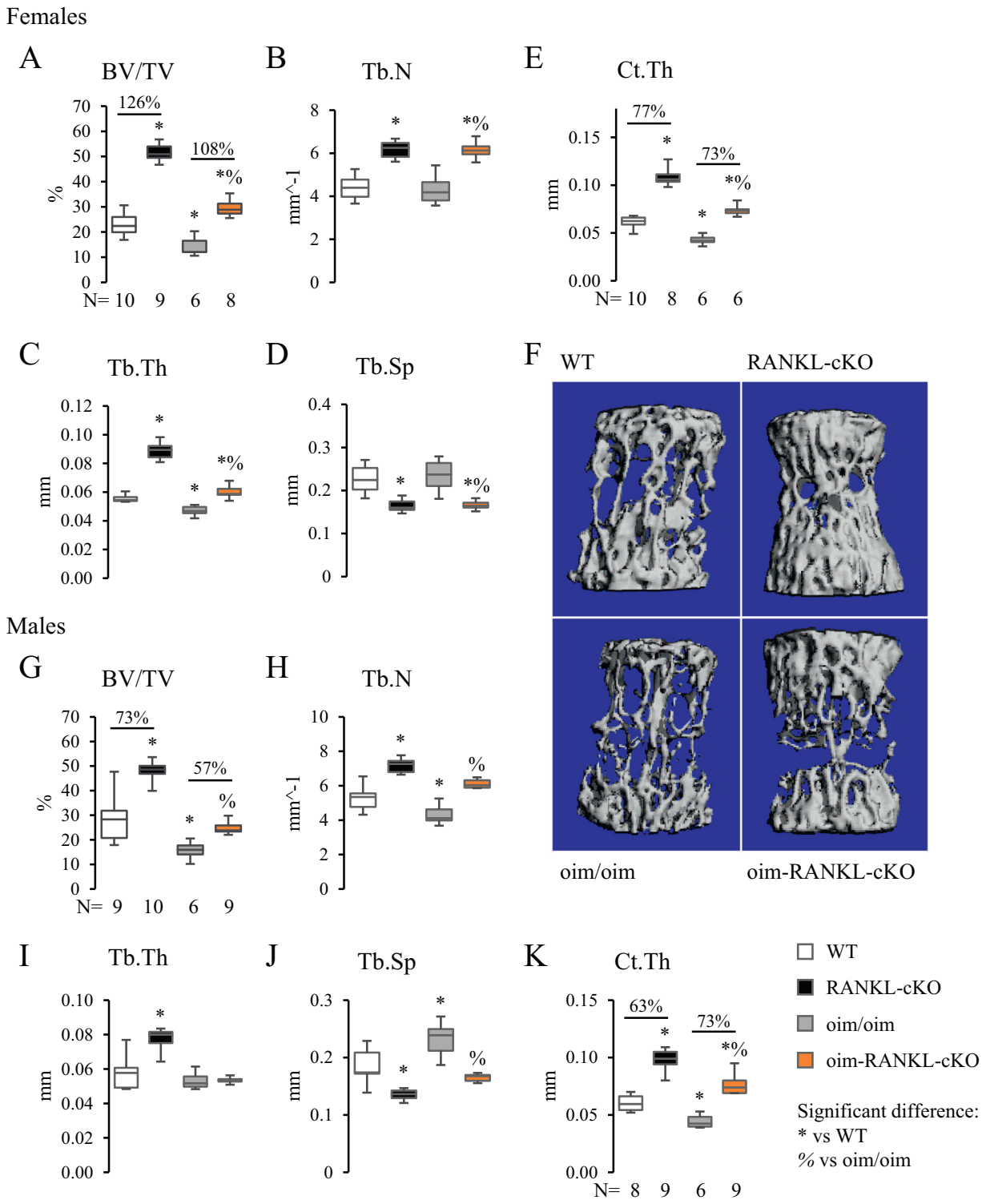

Fig. 3. Static bone parameters of the L4 vertebra measured by micro-CT. Static parameters of the L4 vertebra measured by micro-CT for female (A–F) and male (G–K) 3 month old mice including BV/TV, Tb.N, Tb.Th, Tb.Sp, and cortical thickness (Ct.Th). The Ct.Th was measured at the ventral side of the vertebral body. The N is indicated below the graphs. F. Representative 3D reconstructions of L4 trabecular bone from female mice of each genotype.

Tnfsf11$^{Fl/Fl}$; *Dmp1-Cre* (called "oim-RANKL-cKO" and the subject of this study) and control mice *Col1a2*$^{oim/oim}$; *Tnfsf11*$^{Fl/Fl}$; non-transgenic (equivalent and hereafter referred to as "oim/oim" mice), *Col1a2*$^{+/+}$; *Tnfsf11*$^{Fl/Fl}$; *Dmp1-Cre* ("RANKL-cKO"), and *Col1a2*$^{+/+}$; *Tnfsf11*$^{Fl/Fl}$; non-transgenic (equivalent and hereafter referred to as "WT" control mice as demonstrated by Xiong et al.) (Xiong et al., 2011). The osteocyte-specific deletion of *Tnfsf11* was confirmed using PCR to amplify the region surrounding the recombination site in genomic DNA isolated from multiple tissues (Supplementary Fig. 1A, B). This strategy identified a few mice with improper deletion of *Tnfsf11* exons 3–4 in additional tissues besides bone (7 out of 78 mice tested, 9%, Supplementary Fig. 1B), indicating that the *Dmp1-Cre* transgene can occasionally cause germline deletion; these mice were excluded from our study. Additionally, given the laborious genotyping of the oim mice, we

simplified the process by developing a novel genotyping method to detect the oim allele which is characterized by a single nucleotide deletion in exon 52 of *Col1a2* (see Suppl. Fig. 1C, D). The mice utilized for the subsequent experiments were weighed weekly beginning at 5 weeks of age and until 13 weeks. Throughout this period of time, the oim-RANKL-cKO and oim/oim mice had significantly lower body weight than either the RANKL-cKO or WT mice (Fig. 1B). At 3 months of age the mice were euthanized and all analyses were performed on samples from mice at this age.

3.2. Loss of RANKL in osteocytes in oim mice rescued cancellous bone mass to WT levels

Micro-CT was utilized to study the femur and the L4 lumbar vertebral body in both female and male mice. Micro-CT assessment of cancellous bone in the distal femur revealed that female oim-RANKL-cKO mice have significantly increased bone volume over tissue volume (BV/TV) compared to oim/oim mice (+231%) and reached BV/TV values that were equivalent to those of WT mice albeit significantly lower than RANKL-cKO (Fig. 2A). Also bone trabecular thickness (Tb.Th) and trabecular separation (Tb.Sp) significantly increased and decreased, respectively, in oim-RANKL-cKO compared to oim/oim, while number of trabeculae (Tb.N) did not change (Fig. 2A–E). Notably, the increase in cancellous bone in oim-RANKL-cKO versus oim/oim was similar in magnitude to the increase in RANKL-cKO bone versus WT, the latter was published previously (Xiong et al., 2011). Additionally, cancellous bone extended further into the diaphysis of RANKL-cKO and oim-RANKL-cKO mice compared to WT and oim/oim, respectively (Fig. 2F). In male mice, micro-CT analysis of cancellous bone in the distal femur showed similar results to those observed in females, however, a significant difference between oim-RANKL-cKO and oim/oim was only observed in Tb.Sp (Fig. 2G–J). The power of the statistical analysis of these measurements was impaired by the low number of oim/oim femurs (N = 2) that we were able to collect; the extreme fragility of male long bones and the consequent frequent fractures (before or during harvest) rendered them unusable (see Fig. 5C–D). The micro-CT analysis of the femoral cortical bone at the midshaft showed only a minor increase in cortical thickness (+9%) in oim-RANKL-cKO compared to oim/oim female mice (Supplementary Fig. 2). Other parameters, including bone cross-sectional area (CSA), total CSA and femur length, were only different in mice having the oim/oim mutation compared to controls with normal type I collagen (Supplementary Fig. 2). Femoral cortical bone analysis in male mice was also limited by the small number of intact long bones recovered (N = 1) but it is reported as well in Supplementary Fig. 2 with findings similar to those described in female mice.

Because the analysis of the micro-CT for 3 month-old male femurs was limited by the low N in the oim/oim group, we collected another cohort of mice at 1 month of age. N = 4–5 male femurs were collected from all genotypes, and micro-CT analysis was performed on the cancellous bone of the distal femur and cortical bone at the midshaft (Supplementary Fig. 3). The new results were similar to the data from 3 months of age, except for a few differences. At 3 months of age, the RANKL-cKO mice were significantly different from WT in all cancellous measures (Fig. 2G–J), but at 1 month of age, only BV/TV is significantly different in RANKL-cKO vs WT (Supplementary Fig. 3A). At 3 months of age, the oim/oim mice were significantly different from WT only in Tb.N and Tb.Sp (Fig. 2H, J), but at 1 month of age all parameters were different between these groups (Supplementary Fig. 3A–D). At 3 months of age, the oim-RANKL-cKO mice differed from oim/oim mice only in Tb.Sp (Fig. 2J), but at 1 month they also had significantly increased Tb.N compared to the oim/oim mice (Supplementary Fig. 3B). In the femoral cortical micro-CT analysis, having an increased N for the oim/oim group allowed the detection of significant decreases in Ct.Th, CSA, and Total CSA for the oim/oim group vs the WT and RANKL-cKO groups (Supplementary Fig. 3E–G). Periosteal perimeter, on the other hand, remained unchanged in any group (Supplementary Fig. 3H).

Micro-CT of the L4 vertebra of female mice showed a statistically significant increase in BV/TV, Tb.N, Tb.Th and decrease in Tb.Sp in oim-RANKL-cKO compared to oim/oim mice (Fig. 3A–D). Moreover, the cortical thickness (Ct.Th), measured at the ventral side of the vertebral body, was also significantly increased compared to oim/oim (Fig. 3E). Importantly, BV/TV, Tb.Th, and Ct.Th for oim-RANKL-cKO were not only improved compared to oim/oim but were also significantly increased beyond those of WT mice (Fig. 3A–E). Again, those parameters did not reach the values of the RANKL-cKO mice. Vertebral measurements in male mice provided similar results (Fig. 3G–K), with the exception of trabecular thickness which was not changed. The increase in vertebral cancellous bone in oim-RANKL-cKO versus oim/oim was similar in magnitude to the increase in RANKL-cKO bone versus WT.

3.3. Minimal changes to bone strength in oim-RANKL-cKO compared to oim/oim

To determine whether the gains in femoral and vertebral bone mass in oim-RANKL-cKO would have an effect on bone strength, biomechanical testing was performed on both the femur and the L5 vertebral body. A 3-point bending test on femur revealed no significant changes in elastic modulus, yield stress, or ultimate stress for oim-RANKL-cKO versus oim/oim for either sex (Fig. 4A–F). Since this test measures mainly cortical bone strength at mid-diaphysis, the results are consistent with no significant gain in cortical bone mass in the femur (Supplementary Fig. 2). Interestingly, the loss of RANKL in osteocytes appears to have a more beneficial effect on femur strength in male versus female mice. In fact, while there was an approximately 30% increase in all three parameters in male oim-RANKL-cKO versus oim/oim, yield stress and ultimate stress actually trended downward for female oim-RANKL-cKO mice (Fig. 4 E and F versus B and C). Notably, the yield stress in male femurs from oim-RANKL-cKO was not different compared to that of WT controls (Fig. 4E). However, it is true for both sexes that the groups with the oim mutation had lower values than the groups without the oim mutation. The 3-point bending results are also visualized in stress-strain curves for each sex (Fig. 4G, H).

A compression test on the L5 lumbar vertebral body from female mice was also performed, given the significant gain in trabecular bone mass observed in oim-RANKL-cKO vs oim/oim (> 100%, Fig. 3A). This test showed no significant changes in maximum compression, strain at maximum load, and elastic modulus in oim-RANKL-cKO vs oim/oim (Fig. 4I–K). While the only significant difference detected was a decrease in maximum compression in the oim/oim group compared to WT and RANKL-cKO, the vertebral maximum compression observed in oim-RANKL-cKO was similar to WT levels (Fig. 4I). These data indicate that the large gains in bone mass seen by micro-CT have contributed minimally to overall bone compressive strength.

3.4. Serum analysis of bone turnover markers (BTMs) showed inconsistent results

To assess bone turnover at the systemic level, the serum markers of bone resorption CTX-I and TRAcP5b were measured in all mouse groups. CTX-I was greatly increased in oim/oim and oim-RANKL-cKO compared to WT and RANKL-cKO (Fig. 5A). CTX-I decreased, though not significantly, in mice with osteocyte inactivation of RANKL (34% decrease RANKL-cKO vs WT, 41% decrease oim-RANKL-cKO vs oim/oim). However, serum TRAcP5b, a marker of osteoclast activity, was not significantly changed in any group, although the values trended lower in the RANKL knockout groups (N = 6) (Fig. 5B). Additionally, measurement of TRAcP5b activity was also performed in the sera of 1 month old mice, and no changes were again observed with the exception of a small but significant increase in oim-RANKL-cKO compared to WT and RANKL-cKO groups (Supplementary Fig. 3I). Overall, all the

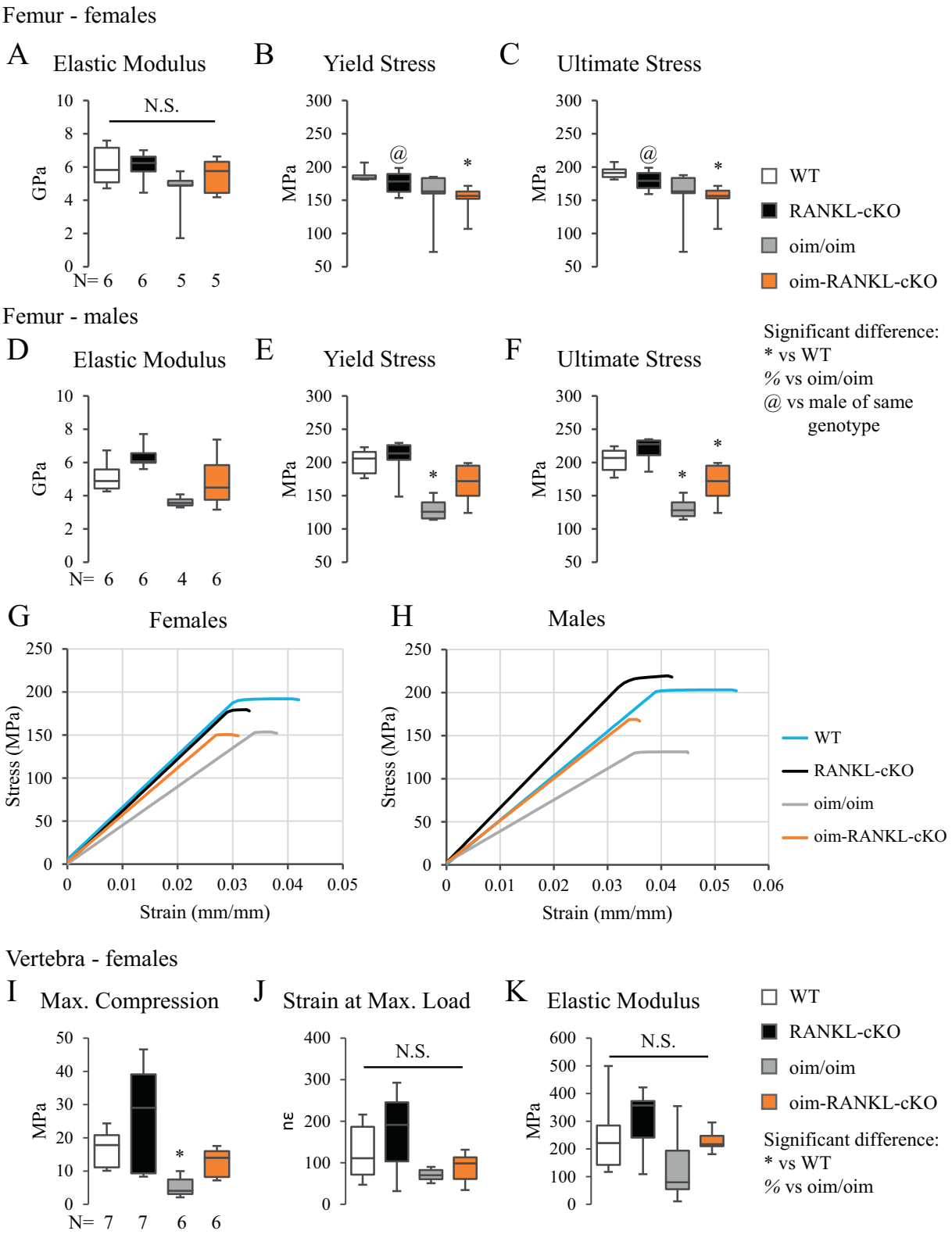

Fig. 4. Femur 3-point bending and vertebral compression biomechanical tests. The biomechanical properties of femurs from 3 month old male and female mice were tested by 3-point bending. The N is indicated below the graphs. Elastic modulus, yield stress, and ultimate stress for females (A–C) and males (D–F) are reported. G, H. Stress-strain curves generated from the average values for each genotype for females (G) and males (H). The elastic modulus is the slope of the linear portion of the curve, the yield stress is the point at which the curve becomes non-linear, and the ultimate stress is the endpoint of the curve (fracture point). I–K. The L5 lumbar vertebral body from 3 month old female mice was subjected to a compression test and the reported parameters are maximum compression, strain at maximum load, and elastic modulus. The N is indicated below the graph in I. N.S. indicates no significant differences.

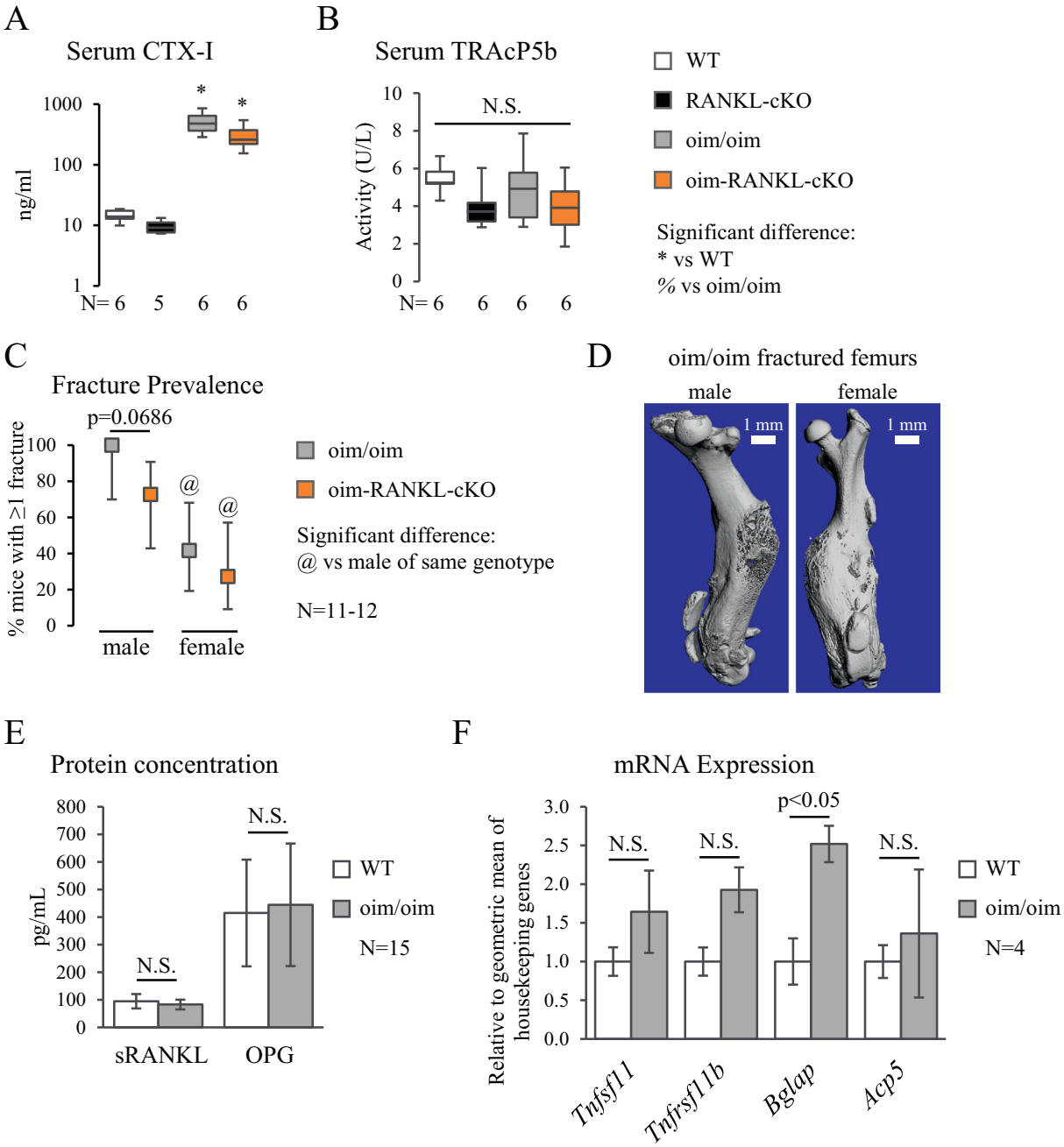

Fig. 5. Bone turnover markers, fracture prevalence, and gene and protein expression analysis. A. Serum levels of bone resorption marker CTX-I measured by enzyme immunoassay. The y-axis is on a logarithmic scale. B. TRAcP5b activity measured by ELISA in serum. C. Fracture prevalence in oim/oim and oim-RANKL-cKO mice (there were no fractures observed in WT or RANKL-cKO mice), plotted as the percent of mice having at least one fracture with the error bars indicating the 95% confidence interval. D. Micro-CT 3D reconstructions of fractured femurs from oim/oim mice (left image is male, right image is female). E. Soluble RANKL (sRANKL) and OPG protein measured in bone marrow supernatant by ELISA. F. The mRNA expression of *Rankl* (*Tnfsf11*), *Opg* (*Tnfrsf11b*), *Ocn* (*Bglap, Bglap2, Bglap3*), and *Trap* (*Acp5*) measured by real-time PCR on osteocyte-enriched cDNA samples from mouse femur and tibia. Values are normalized to the geometric mean of five housekeeping genes. N.S. indicates no significant differences. The N for each panel is indicated below or to the side of the graph.

groups had higher levels of TRAcP5b activity at 1 month of age vs 3 months, as expected in growing mice.

Because oim/oim mice are known to suffer spontaneous fractures, the number of fractured femora and tibiae per mouse at the time of euthanasia were recorded and analyzed. Fractures were significantly more common in male oim/oim and oim-RANKL-cKO than female mice (Fig. 5C). No fractures were observed in any WT or RANKL-cKO mice. Strikingly, 100% of male oim/oim mice in our study had fractures, but only 72.7% of male oim-RANKL-cKO mice had fractures (an almost significant decrease, $p = 0.0686$) (Fig. 5C–D). Because of the conflicting serum biomarkers results (i.e. high CTX-I but unchanged TRAcP5b) and previous data from the literature on the oim mice, soluble RANKL (sRANKL) and OPG protein concentrations in bone marrow supernatant were analyzed in the original oim mouse strain that was used for the genetic cross described in this study. The results showed no changes in oim mice compared to WT (Fig. 5E). Furthermore, the relative mRNA expression of *Tnfsf11* (encoding RANKL), *Tnfrsf11b* (encoding OPG), and *Acp5* (encoding TRAP5b) in osteocyte-enriched bone from oim and WT mice were not different (Fig. 5F). Only *Bglap* (encoding Osteocalcin, OCN), a marker of osteoblast function,

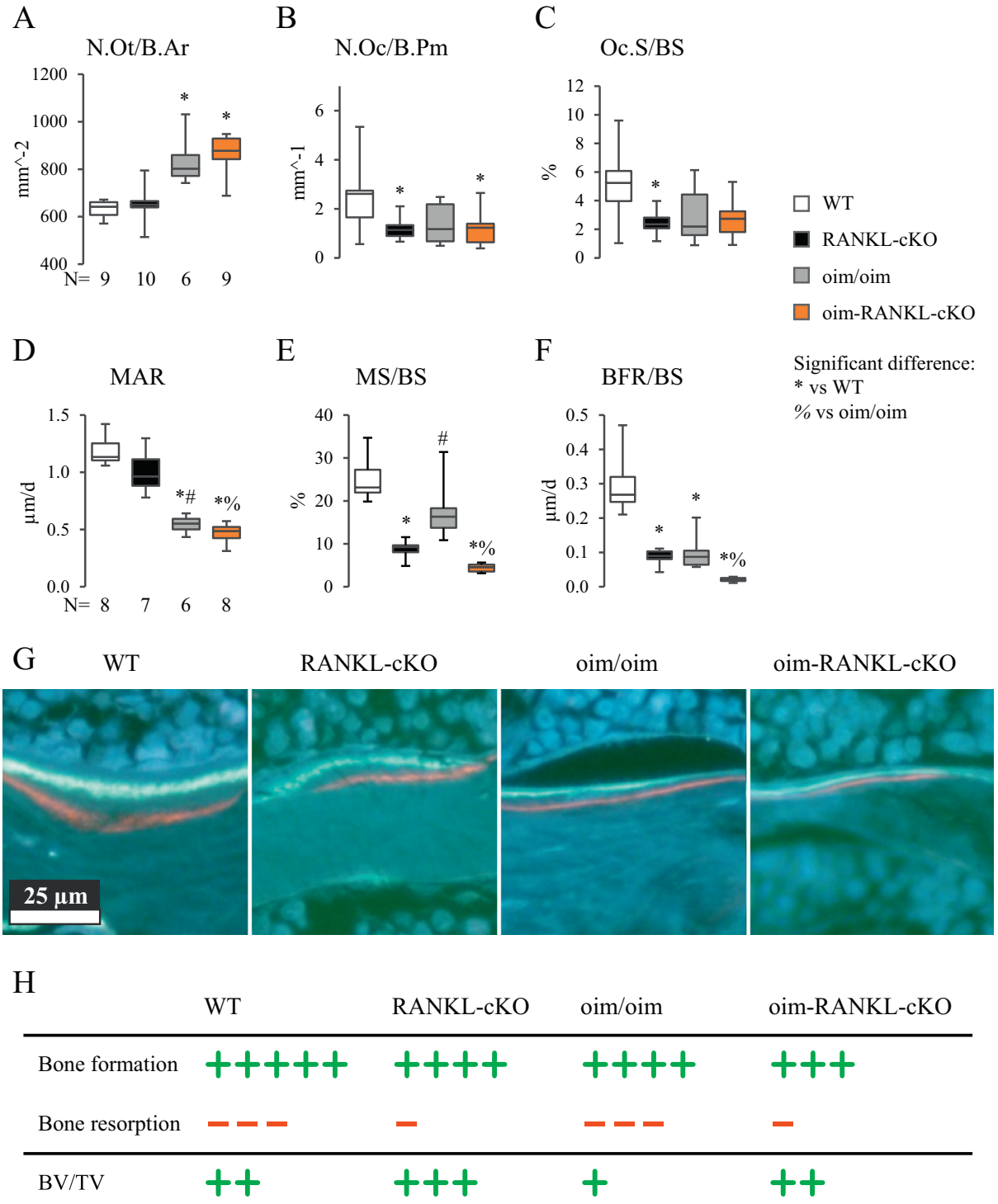

Fig. 6. Cell numbers and dynamic parameters of bone formation measured by bone histomorphometry in the lumbar spine. A. Osteocyte number per bone area (N.Ot/B.Ar), B. osteoclast number per bone perimeter (N.Oc/B.Pm), and C. osteoclast surface expressed as percentage of bone surface (Oc.S/BS) were measured in the cancellous bone of the lumbar spine from male mice. Also measured on a subset of these same mice, D. mineral apposition rate (MAR), E. mineralizing surfaces per bone surfaces (MS/BS) and F. bone formation rate per bone surface (BFR/BS). Significant differences are indicated in each panel, and the N is indicated below the graphs. G. Representative histological images of fluorescently double-labeled cancellous bone surfaces in the lumbar spine. H. Schematic interpretation of the histomorphometry results expressed as bone formation (green plus signs) and bone resorption (red dashes) and their net effect on BV/TV. (For interpretation of the references to color in this figure legend, the reader is referred to the web version of this article.)

was slightly but significantly up-regulated in oim vs WT osteocyte-enriched bone (Fig. 5F). Taken together, the increased CTX-I serum levels and *Ocn* gene expression would suggest high bone turnover while normal TRAcP5b, RANKL, OPG (and the RANKL/OPG ratio) indicate normal bone turnover.

3.5. Bone histomorphometry indicated that oim/oim mice do not have high bone turnover in the lumbar spine

To further investigate the discrepancy derived from the BTMs, histological analysis of the lumbar spine from male mice was performed to

assess what changes have occurred at the cellular level in oim/oim and oim-RANKL-cKO mice. High osteocyte density, a feature commonly seen in OI (Sarathchandra et al., 2000), was clearly detected in the oim/oim and oim-RANKL-cKO mice (Fig. 6A). Because oim/oim mice were previously described to have high bone turnover and increased osteoblast and osteoclasts parameters (Kalajzic et al., 2002), the expectation was to replicate similar findings in the oim-RANKL-flox (oim/oim) mice and assess if the RANKL deletion in osteocyte would significantly modify them. While we detected low osteoclast numbers and surfaces in the oim-RANKL-cKO and RANKL-cKO groups compared to WT unexpectedly, neither osteoclast numbers nor surfaces were elevated in the oim/oim group (Fig. 6B–C). Moreover, the oim/oim mice had surprisingly low mineral apposition rate (MAR) and mineralizing surfaces (MS/BS) resulting in a significant decrease in bone formation rate (BFR/BS) compared to WT (Fig. 6D–H). As expected these parameters were decreased even further in oim-RANKL-cKO (Fig. 6D–H). Thus, at least in the spine at 3 months of age, oim/oim mice do not show signs of high bone turnover, and oim-RANKL-cKO, while having similar osteoclast numbers and surfaces, show further reduction in MAR and BFR compared to oim/oim.

4. Discussion

In recent years, osteocytes have been recognized as important choreographers of skeletal homeostasis (Manolagas and Parfitt, 2010). Importantly, osteocyte apoptosis or their dysregulation has been implicated in several diseases, including osteoporosis, osteoarthritis, osteomalacia, and others (Dallas et al., 2013). Recent work also showed that hypertrophic chondrocytes and osteocytes are a major source of RANKL during mineralized cartilage resorption and adult bone remodeling, respectively (Xiong et al., 2011; Nakashima et al., 2011). Increased osteocyte density has been observed in both human and murine OI bone (Chipman et al., 1993; Sarathchandra et al., 2000), however how osteocytes embedded in a matrix of abnormal type I collagen may contribute to OI pathogenesis is poorly understood. In this study we investigated the contribution of osteocyte-produced RANKL to low bone mass and biomechanical, serum and cellular parameters in a mouse model of OI. To do this we chose the oim/oim mouse (osteogenesis imperfecta mouse), a mouse model of moderate to severe OI which produces α1(I) homotrimers and is characterized by low bone mass, spontaneous fractures and was shown previously to have high osteoblast and osteoclast surfaces (Chipman et al., 1993; Kalajzic et al., 2002). Oim/oim mice with a concomitant loss of RANKL in osteocytes at 3 months of age had large gains in cancellous bone mass of the distal femur (BV/TV +231% for females, +137% for males) and the L4 vertebral body (+108% for females, +57% for males) compared to oim/oim mice. In both instances the gain in cancellous bone mass raised the BV/TV values of oim-RANKL-cKO mice to similar or higher level to those of WT mice. The increase in cancellous bone volume in oim-RANKL-cKO mice versus oim/oim was similar to that observed in RANKL-cKO versus WT, the latter was reported previously and replicated in this study (Xiong et al., 2011).

The micro-CT analysis of the cortical bone thickness showed a small, non-significant improvement, in the femur but a significant increase in the L4 lumbar vertebral body (+73%, measured at the ventral side) of oim-RANKL-cKO compared to oim/oim. Therefore, the primary effects of the genetic deletion of *Tnfsf11* in osteocytes are in cancellous bone of the long bone and spine and in vertebral cortical thickness, in both sexes. It is also clear that, while our genetic intervention was effective at increasing bone mass, it did not address the underlying collagen defect and the weakened material properties. In fact, the increase in bone mass provided minimal improvement in the bone biomechanical properties and this is similar to a previous report where the treatment of oim/oim mice with RANK-Fc caused no significant changes in biomechanical parameters (Bargman et al., 2012). The genetic loss of RANKL in osteocytes provided no improvement in overall bone strength since the reduction in number of fractures did not reach statistical significance. Interestingly, long bones in female mice fractured significantly less in presence of the oim mutation compared to male long bones suggesting a clear sexual dimorphism in fracture susceptibility (Fig. 5C). This sexual dimorphism is also supported by the 3-point bending test data (Fig. 4A–F), where oim/oim female femurs had similar elastic modulus, yield stress and ultimate stress to WT controls, unlike males of the same genotype.

Bone histomorphometry analysis was performed on L3-L5 male vertebral bodies in the lumbar spine. This site was selected because, even in an OI mouse model such as the oim/oim in a pure C57BL/6 genetic background (as used in this study), there is still abundant cancellous bone for measurement compared to what was observed in the oim/oim long bone in a mixed genetic background (Vanleene and Shefelbine, 2013). The results surprisingly showed that the oim/oim mice have osteoclast numbers and surfaces similar to WT, and low mineral apposition and bone formation rate compared to WT mice. This is different from what was published before, though in tibiae of oim/oim mice (Kalajzic et al., 2002). The additional loss of RANKL from osteocytes in the oim-RANKL-cKO and RANKL-cKO mice further diminished the MAR and BFR/BS compared to oim/oim and WT mice, respectively and as expected. Our interpretation of the histomorphometry data from the vertebral cancellous bone, together with the data shown in Fig. 3, is summarized in Fig. 6H. Oim/oim mice have normal bone resorption but decreased bone formation which makes them significantly osteopenic. The loss of osteocyte-derived RANKL in oim/oim mice further decreases bone formation rate but may also reduce bone resorption compared to oim/oim, although osteoclast parameters were not different given the already low median values of osteoclasts in the oim/oim mice and the variability in those values. The net effect of this is that oim-RANKL-cKO mice regain WT levels of bone mass. The mechanisms underlying the higher bone mass in the oim-RANKL-cKO mice compared to oim/oim mice are uncertain. However, based on the known roles of RANKL, it seems likely that reduced bone resorption must play a role. While we did not observe a decrease in osteoclast number in the oim-RANKL-cKO mice compared to oim/oim mice, we did observe a reduction in the bone formation rate which may reflect a decrease in bone resorption due to the coupling of the former to the latter.

Notably, the analysis of circulating markers of bone turnover in the serum showed greatly increased levels of CTX-I in oim/oim (consistent with previous findings from others (Matthews et al., 2017)) and oim-RANKL-cKO mice compared to WT and RANKL-cKO. However, no overall significant changes in TRAcP5b activity were detected among the four genotypes. The lack of difference in TRAcP5b activity between WT and oim/oim mice confirms identical results described by Bargman et al. at 14 weeks of age (Bargman et al., 2012) and was also shown at 1 month of age (see Supplementary Fig. 3I). Moreover, there were no changes in sRANKL and OPG protein concentrations in bone marrow supernatant, nor changes in *Tnfsf11*, *Tnfrsf11b*, and *Acp5* gene expression in osteocyte-enriched cortical bone as detected in the original oim/oim (without the RANKL-flox allele) versus WT mice. Collectively, the bone histomorphometric data indicate that, at least in the lumbar spine at 3 months of age, the oim/oim mice do not show cellular signs of high bone turnover. This is supported by the unchanged serum levels of TRAcP5b activity and the protein and mRNA expression results. Only the high levels of CTX-I would point to a high bone turnover phenotype in the oim/oim compared to the WT mice. It is well known that mice homozygous for the oim mutation spontaneously fracture, especially in the long bones and in the tail vertebrae (Chipman et al., 1993; Bargman et al., 2012). Therefore, the explanation for the increased, systemic level of CTX-I in oim/oim mice may derive from the accounted (in long bones of the leg) or unaccounted spontaneous bone fractures that are being remodeled during bone healing. The remodeling fracture calluses are known to increase systemic CTX-I levels for several weeks post-fracture (Stoffel et al., 2007; Cox et al., 2010). It is unclear though why

TRAcP5B activity remains unchanged. In addition, oim/oim mice make homotrimeric $\alpha1(I)_3$ instead of $\alpha1(I)_2\alpha2(I)$ collagen fibrils. Thus the enzyme immunoassay (RatLaps), based on the competitive binding of a polyclonal antibody against the soluble antigen EKSQDGGR derived from the C-telo-peptide of α1(I), could overestimate the total content of CTX-I in oim/oim compared to WT mice. Moreover, because type I collagen homotrimers in oim/oim mice are expressed in several tissues of the body, it is also possible that the ECM turnover may be ubiquitously increased and thus result in increased type I collagen degradation products in the serum. Ultimately, our data suggest that CTX-I values in serum of oim/oim mice should be interpreted cautiously.

As mentioned earlier, it was previously reported that oim/oim mice have high bone turnover, based on high osteoblast, osteoclast numbers and high BFR in the tibia at 3 months of age, and high urinary deoxypyridinoline crosslinks (Kalajzic et al., 2002). Subsequent work showed an increase in immature but not mature osteoblasts on endocortical surfaces of femurs at 3 months of age (Li et al., 2010). Conversely, in vitro assays clearly showed an increased ability of oim/oim osteoblasts to support osteoclastogenesis (Li et al., 2010), and of oim/oim osteoclasts to have increased resorptive activity on bone slices (Zhang et al., 2007). The differences between these previous studies and the present could be accounted for by in vitro versus ex vivo studies, the different sites analyzed by bone histomorphometry or fluorescent lineage tracing, i.e. long bones vs the spine, and also the different genetic background, i.e. mixed in the previous studies vs pure C57BL6 in the present. A study which aimed to determine the phenotypic variance in severity due to the genetic background in the oim/oim mouse concluded that the genetic background plays a significant role in the severity of the oim mutation but that the primary determinants were the presence of the oim mutation and the age of the mice (Carleton et al., 2008). Importantly, this study also reported no differences in serum pyridinoline crosslinks in oim/oim compared to WT, further suggesting normal bone turnover in the former (Carleton et al., 2008). Although high bone turnover was reported in children and adults with OI (Rauch et al., 2000; Baron et al., 1983; Braga et al., 2004), it is not consistently present in mouse models of OI. The *Col1a1*$^{+/Jrt}$ model has shown signs of high bone turnover in three different studies (Chen et al., 2014; Roschger et al., 2014; Boraschi-Diaz et al., 2017). However, two other commonly used OI models, the *Col1a2*$^{+/G610C}$ "Amish" and the *Col1a1*$^{+/G349C}$ "BrtlIV" mice, have been reported with either mostly normal turnover (*Col1a2*$^{+/G610C}$ "Amish" mice (Jacobsen et al., 2014)) or inconsistent results, respectively (*Col1a1*$^{+/G349C}$ "BrtlIV" mice (Uveges et al., 2008; Uveges et al., 2009; Sinder et al., 2013; Sinder et al., 2015; Sinder et al., 2014)). Bone turnover data is sparse for models of recessive OI due to non-collagenous mutations. The most studied of these is the *CrtapKO* mouse, which was shown to have either high turnover (Grafe et al., 2014), or normal resorption and low bone formation (Morello et al., 2006).

The use of denosumab, a humanized monoclonal antibody against RANKL, was shown to be an effective and apparently safe treatment option for children with OI type VI, showing increased BMD, mobility, normalization of vertebral shape and fracture rate reduction (Hoyer-Kuhn et al., 2014). However, the genetic global suppression of RANKL in mice is deleterious for the proper development and maturation of the immune system (Ferrari-Lacraz and Ferrari, 2011) and this leaves open questions about the potential consequences of denosumab use in young children. The results of our study suggest that a bone targeted denosumab formulation instead of systemic could represent an equally effective therapy for increasing BMD while not impacting other systems.

In conclusion, our study has shown that, upon further examination, oim/oim mice do not have high bone turnover and their low bone mass is due to defective bone formation and not increased bone resorption. Furthermore, osteocyte-derived RANKL is also important in OI and its loss produces similar positive effects on the skeleton compared to the systemic inhibition of RANKL.

Supplementary data to this article can be found online at https://doi.org/10.1016/j.bonr.2018.06.008.

Transparency document

The Transparency document associated this article can be found, in online version.

Acknowledgements

The authors would like to thank Igor Gubrij for embedding and staining the spines used for histomorphometry, Dr. Larry Suva for training on the micro-CT, Stuart Berryhill for training on micro-CT, histomorphometry, and biomechanics, Drs. Charlotte Phillips and Sarah Dallas for providing the oim mice in a pure C57Bbl/6 genetic background, and Dr. Robert Jilka for helpful discussion.

Funding

This work was supported in part by NIH funds from NIAMS (R01 AR060823-01A1 to RM) and NIGMS (P20GM125503 to CAO); by University of Arkansas for Medical Sciences institutional funds; and by private donations of Mr. and Mrs. Brent Jones.

References

Bargman, R., Posham, R., Boskey, A.L., Dicarlo, E., Raggio, C., Pleshko, N., 2012. Comparable outcomes in fracture reduction and bone properties with RANKL inhibition and alendronate treatment in a mouse model of osteogenesis imperfecta. Osteoporos. Int. 23, 1141–1150.

Baron, R., Gertner, J.M., Lang, R., Vignery, A., 1983. Increased bone turnover with decreased bone formation by osteoblasts in children with osteogenesis imperfecta tarda. Pediatr. Res. 17, 204–207.

Bellido, T., 2014. Osteocyte-driven bone remodeling. Calcif. Tissue Int. 94, 25–34.

van Bezooijen, R.L., Roelen, B.A., Visser, A., van der Wee-Pals, L., de Wilt, E., Karperien, M., et al., 2004. Sclerostin is an osteocyte-expressed negative regulator of bone formation, but not a classical BMP antagonist. J. Exp. Med. 199, 805–814.

Boraschi-Diaz, I., Tauer, J.T., El-Rifai, O., Guillemette, D., Lefebvre, G., Rauch, F., et al., 2017. Metabolic phenotype in the mouse model of osteogenesis imperfecta. J. Endocrinol. 234, 279–289.

Bouxsein, M.L., Boyd, S.K., Christiansen, B.A., Guldberg, R.E., Jepsen, K.J., Muller, R., 2010. Guidelines for assessment of bone microstructure in rodents using micro-computed tomography. J. Bone Miner. Res. 25, 1468–1486.

Braga, V., Gatti, D., Rossini, M., Colapietro, F., Battaglia, E., Viapiana, O., et al., 2004. Bone turnover markers in patients with osteogenesis imperfecta. Bone 34, 1013–1016.

Carleton, S.M., McBride, D.J., Carson, W.L., Huntington, C.E., Twenter, K.L., Rolwes, K.M., et al., 2008. Role of genetic background in determining phenotypic severity throughout postnatal development and at peak bone mass in Col1a2 deficient mice (oim). Bone 42, 681–694.

Chen, F., Guo, R., Itoh, S., Moreno, L., Rosenthal, E., Zappitelli, T., et al., 2014. First mouse model for combined osteogenesis imperfecta and Ehlers-Danlos syndrome. J. Bone Miner. Res. 29, 1412–1423.

Chipman, S.D., Sweet, H.O., McBride Jr., D.J., Davisson, M.T., Marks Jr., S.C., Shuldiner, A.R., et al., 1993. Defective pro alpha 2(I) collagen synthesis in a recessive mutation in mice: a model of human osteogenesis imperfecta. Proc. Natl. Acad. Sci. U. S. A. 90, 1701–1705.

Cox, G., Einhorn, T.A., Tzioupis, C., Giannoudis, P.V., 2010. Bone-turnover markers in fracture healing. J. Bone Joint Surg. Br. 92, 329–334.

Dallas, S.L., Prideaux, M., Bonewald, L.F., 2013. The osteocyte: an endocrine cell … and more. Endocr. Rev. 34, 658–690.

Dempster, D.W., Compston, J.E., Drezner, M.K., Glorieux, F.H., Kanis, J.A., Malluche, H., et al., 2013. Standardized nomenclature, symbols, and units for bone histomorphometry: a 2012 update of the report of the ASBMR Histomorphometry Nomenclature Committee. J. Bone Miner. Res. 28, 2–17.

Ferrari-Lacraz, S., Ferrari, S., 2011. Do RANKL inhibitors (denosumab) affect inflammation and immunity? Osteoporos. Int. 22, 435–446.

Fujiwara, Y., Piemontese, M., Liu, Y., Thostenson, J.D., Xiong, J., O'Brien, C.A., 2016. RANKL (receptor activator of NFkappaB ligand) produced by osteocytes is required for the increase in B cells and bone loss caused by estrogen deficiency in mice. J. Biol. Chem. 291, 24838–24850.

Genetics Home Reference Osteogenesis Imperfecta. U.S. Department of Health & Human Services. Accessed on: November 12, 2017. Available from: https://ghr.nlm.nih.gov/condition/osteogenesis-imperfecta#statistics.

Grafe, I., Yang, T., Alexander, S., Homan, E.P., Lietman, C., Jiang, M.M., et al., 2014. Excessive transforming growth factor-beta signaling is a common mechanism in osteogenesis imperfecta. Nat. Med. 20, 670–675.

Hoyer-Kuhn, H., Netzer, C., Koerber, F., Schoenau, E., Semler, O., 2014. Two years' experience with denosumab for children with osteogenesis imperfecta type VI.

Orphanet J. Rare Dis. 9, 145.
Jacobsen, C.M., Barber, L.A., Ayturk, U.M., Roberts, H.J., Deal, L.E., Schwartz, M.A., et al., 2014. Targeting the LRP5 pathway improves bone properties in a mouse model of osteogenesis imperfecta. J. Bone Miner. Res. 29, 2297–2306.
Joeng, K.S., Lee, Y.C., Lim, J., Chen, Y., Jiang, M.M., Munivez, E., et al., 2017. Osteocyte-specific WNT1 regulates osteoblast function during bone homeostasis. J. Clin. Invest. 127, 2678–2688.
Kalajzic, I., Terzic, J., Rumboldt, Z., Mack, K., Naprta, A., Ledgard, F., et al., 2002. Osteoblastic response to the defective matrix in the osteogenesis imperfecta murine (oim) mouse. Endocrinology 143, 1594–1601.
Li, H., Jiang, X., Delaney, J., Franceschetti, T., Bilic-Curcic, I., Kalinovsky, J., et al., 2010. Immature osteoblast lineage cells increase osteoclastogenesis in osteogenesis imperfecta murine. Am. J. Pathol. 176, 2405–2413.
Lu, Y., Xie, Y., Zhang, S., Dusevich, V., Bonewald, L.F., Feng, J.Q., 2007. DMP1-targeted Cre expression in odontoblasts and osteocytes. J. Dent. Res. 86, 320–325.
Manolagas, S.C., Parfitt, A.M., 2010. What old means to bone. Trends Endocrinol. Metab. 21, 369–374.
Marini, J.C., Forlino, A., Bachinger, H.P., Bishop, N.J., Byers, P.H., Paepe, A., et al., 2017. Osteogenesis imperfecta. Nat. Rev. Dis. Prim. 3, 17052.
Matthews, B.G., Roeder, E., Wang, X., Aguila, H.L., Lee, S.K., Grcevic, D., et al., 2017. Splenomegaly, myeloid lineage expansion and increased osteoclastogenesis in osteogenesis imperfecta murine. Bone 103, 1–11.
Morello, R., Bertin, T.K., Chen, Y., Hicks, J., Tonachini, L., Monticone, M., et al., 2006. CRTAP is required for prolyl 3-hydroxylation and mutations cause recessive osteogenesis imperfecta. Cell 127, 291–304.
Nakashima, T., Hayashi, M., Fukunaga, T., Kurata, K., Oh-Hora, M., Feng, J.Q., et al., 2011. Evidence for osteocyte regulation of bone homeostasis through RANKL expression. Nat. Med. 17, 1231–1234.
O'Brien, C.A., Nakashima, T., Takayanagi, H., 2013. Osteocyte control of osteoclastogenesis. Bone 54, 258–263.
Piemontese, M., Xiong, J., Fujiwara, Y., Thostenson, J.D., O'Brien, C.A., 2016. Cortical bone loss caused by glucocorticoid excess requires RANKL production by osteocytes and is associated with reduced OPG expression in mice. Am. J. Physiol. Endocrinol. Metab. 311, E587–E593.
Rauch, F., Travers, R., Parfitt, A.M., Glorieux, F.H., 2000. Static and dynamic bone histomorphometry in children with osteogenesis imperfecta. Bone 26, 581–589.
Roschger, A., Roschger, P., Keplingter, P., Klaushofer, K., Abdullah, S., Kneissel, M., et al., 2014. Effect of sclerostin antibody treatment in a mouse model of severe osteogenesis imperfecta. Bone 66, 182–188.
Sarathchandra, P., Pope, F.M., Kayser, M.V., Ali, S.Y., 2000. A light and electron microscopic study of osteogenesis imperfecta bone samples, with reference to collagen chemistry and clinical phenotype. J. Pathol. 192, 385–395.
Sinder, B.P., Eddy, M.M., Ominsky, M.S., Caird, M.S., Marini, J.C., Kozloff, K.M., 2013. Sclerostin antibody improves skeletal parameters in a Brtl/+ mouse model of osteogenesis imperfecta. J. Bone Miner. Res. 28, 73–80.
Sinder, B.P., White, L.E., Salemi, J.D., Ominsky, M.S., Caird, M.S., Marini, J.C., et al., 2014. Adult Brtl/+ mouse model of osteogenesis imperfecta demonstrates anabolic response to sclerostin antibody treatment with increased bone mass and strength. Osteoporos. Int. 25, 2097–2107.
Sinder, B.P., Salemi, J.D., Ominsky, M.S., Caird, M.S., Marini, J.C., Kozloff, K.M., 2015. Rapidly growing Brtl/+ mouse model of osteogenesis imperfecta improves bone mass and strength with sclerostin antibody treatment. Bone 71, 115–123.
Stoffel, K., Engler, H., Kuster, M., Riesen, W., 2007. Changes in biochemical markers after lower limb fractures. Clin. Chem. 53, 131–134.
Suva, L.J., Hartman, E., Dilley, J.D., Russell, S., Akel, N.S., Skinner, R.A., et al., 2008. Platelet dysfunction and a high bone mass phenotype in a murine model of platelet-type von Willebrand disease. Am. J. Pathol. 172, 430–439.
Uveges, T.E., Collin-Osdoby, P., Cabral, W.A., Ledgard, F., Goldberg, L., Bergwitz, C., et al., 2008. Cellular mechanism of decreased bone in Brtl mouse model of OI: imbalance of decreased osteoblast function and increased osteoclasts and their precursors. J. Bone Miner. Res. 23, 1983–1994.
Uveges, T.E., Kozloff, K.M., Ty, J.M., Ledgard, F., Raggio, C.L., Gronowicz, G., et al., 2009. Alendronate treatment of the brtl osteogenesis imperfecta mouse improves femoral geometry and load response before fracture but decreases predicted material properties and has detrimental effects on osteoblasts and bone formation. J. Bone Miner. Res. 24, 849–859.
Vanleene, M., Shefelbine, S.J., 2013. Therapeutic impact of low amplitude high frequency whole body vibrations on the osteogenesis imperfecta mouse bone. Bone 53, 507–514.
Xiong, J., Onal, M., Jilka, R.L., Weinstein, R.S., Manolagas, S.C., O'Brien, C.A., 2011. Matrix-embedded cells control osteoclast formation. Nat. Med. 17, 1235–1241.
Xiong, J., Piemontese, M., Thostenson, J.D., Weinstein, R.S., Manolagas, S.C., O'Brien, C.A., 2014. Osteocyte-derived RANKL is a critical mediator of the increased bone resorption caused by dietary calcium deficiency. Bone 66, 146–154.
Ye, S., Dhillon, S., Ke, X., Collins, A.R., Day, I.N., 2001. An efficient procedure for genotyping single nucleotide polymorphisms. Nucleic Acids Res. 29, E88-88.
Zhang, H., Doty, S.B., Hughes, C., Dempster, D., Camacho, N.P., 2007. Increased resorptive activity and accompanying morphological alterations in osteoclasts derived from the oim/oim mouse model of osteogenesis imperfecta. J. Cell. Biochem. 102, 1011–1020.